Au_{25} cluster-loaded $SrTiO_3$ water-splitting photocatalyst; preparation and elucidation of the effect of cocatalyst refinement on photocatalytic activity

Wataru Kurashige,[1] Rina Kumazawa,[1] Yutaro Mori,[1] and Yuichi Negishi*,[1,2]
1. Department of Applied Chemistry, Faculty of Science, Tokyo University of Science, 1-3 Kagurazaka, Shinjuku-ku, Tokyo 162-8601, Japan.
2. Photocatalysis International Research Center, Tokyo University of Science, 2641 Yamazaki, Noda, Chiba 278-8510, Japan.
E-mail:negishi@rs.kagu.tus.ac.jp

Abstract: Water-splitting photocatalysts have attracted much attention for decades as materials to produce clean and renewable hydrogen (H_2) as a fuel. In this study, we succeeded in precisely loading ultrafine gold cocatalyst particles (Au_{25} clusters) on the water-splitting photocatalyst $SrTiO_3$ using glutathionate-protected Au_{25} clusters as a precursor. Photocatalysis experiments using the obtained photocatalyst revealed that the ultra-miniaturization of the Au cocatalyst on $SrTiO_3$ improves its water-splitting activity. The main reason for this improvement was attributed to the acceleration of the H_2-evolution reaction caused by the ultra-miniaturization of the cocatalyst. This effect of refining the cocatalyst differs from that of Au-loaded $BaLa_4Ti_4O_{15}$. These results demonstrate that the effect of ultra-miniaturization of the cocatalyst on photocatalytic activity varies depending on the photocatalyst.
Keywords: water-splitting photocatalyst; gold cocatalyst; $SrTiO_3$; water-splitting activity; $BaLa_4Ti_4O_{15}$

1. Introduction

Efficient use of energy resources and global environmental conservation are major tasks imposed on humanity that require urgent attention. Hydrogen (H_2) can be stored, transported, and releases a large amount of energy when combusted. In addition, it can be converted to electric power via a fuel cell. Furthermore, only water (H_2O) remains after combustion, which means that energy-release from H_2 does not impose any environmental burden. These characteristics make H_2 promising as a new energy source to solve energy and environmental problems.

At present, most H_2 is manufactured by refining fossil resources. In these methods, in addition to consuming fossil-fuel resources, carbon dioxide is produced as a by-product. Therefore, continuing to manufacture H_2 by refining fossil fuels does not lead to solutions to both energy and environmental problems. In contrast, the water-splitting photocatalytic reaction that generates H_2 from H_2O using solar energy (sunlight) can generate H_2 as truly clean and renewable energy.[1] Therefore, water-splitting photocatalysts (Scheme 1(a)) have attracted much attention for many years.[2–15] However, further improvements are needed to make these photocatalysts suitable for practical use.

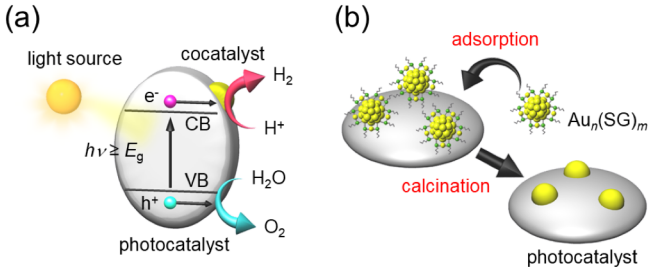

Scheme 1. (a) Schematic of photocatalytic water splitting using a one-step photoexcitation system. CB, conduction band; VB, valence band; E_g, band gap. (b) Schematic of the method used to load highly regulated metal clusters on a photocatalyst surface.

Recent studies demonstrated that control of the active site (supported metal nanocluster; Scheme 1(a)) is an effective way to achieve highly active water-splitting semiconductor photocatalysts.[2,7,8] This control may be accomplished using ligand-protected metal nanoclusters[16–39] as precursors.[37–39] In this approach, size-

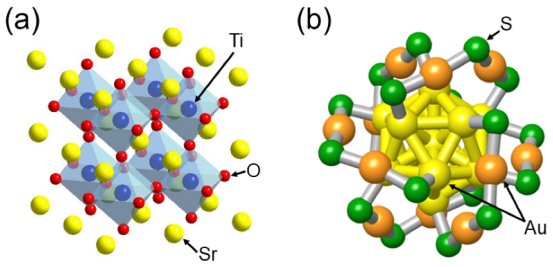

Scheme 2. Structures (a) reported for $SrTiO_3$[44] and (b) proposed for $Au_{25}(SG)_{18}$[19]. In (b), only Au and S atoms are shown for clarity.

controlled metal clusters fabricated by liquid-phase synthesis are adsorbed on the photocatalyst and then the ligands are removed by calcination. As a result, the metal clusters are loaded on the photocatalyst in a controlled manner (Scheme 1(b)).[37–39] Using this approach, we have precisely loaded 25-atom gold clusters (hereinafter referred to as Au_{25} clusters) with a size of only ~1.1 nm on $BaLa_4Ti_4O_{15}$[40], one of the most advanced water-splitting photocatalysts to date.[41–43] Furthermore, studies on the thus-obtained photocatalyst ($Au_{25}/BaLa_4Ti_4O_{15}$) revealed that ultra-miniaturization of the Au cocatalyst accelerates both the H_2 generation and inhibition reactions. Thus, we demonstrated that to create a highly active photocatalyst utilizing the unique characteristics of the ultrafine Au-cluster cocatalyst, it is necessary to form a layer[2,8,9,12–15,37–39] that suppresses the inhibition reaction on the Au cocatalyst.[43] However, the following two questions remain concerning the effective photocatalyst activation by this approach: (1) Is it possible to use this approach to precisely load extremely fine Au-cocatalyst particles on other photocatalysts? (2) Does ultra-miniaturization of the Au cocatalyst have the same effect on other photocatalysts as it does on $BaLa_4Ti_4O_{15}$?

$SrTiO_3$ (Scheme 2(a))[44] promotes the water-splitting reaction when irradiated with ultraviolet (UV) light, similar to $BaLa_4Ti_4O_{15}$. In addition, Au can function as a cocatalyst for $SrTiO_3$.[45] The band gap of $SrTiO_3$ can be controlled by doping with heteroelements (Rh, Cr) and the obtained heteroelement-doped $SrTiO_3$ ($SrTiO_3$:Rh, $SrTiO_3$:Cr) is also frequently used as a H_2-evolution photocatalyst in the visible-light-responsive water-splitting reaction using the Z-scheme.[3–8,11] Thus, herein we use $SrTiO_3$ to answer the above two questions. We found that the size of the Au cocatalyst on $SrTiO_3$ can be strictly controlled within a very narrow region by the method depicted in Scheme 1(b). The water-splitting activity of Au-loaded $SrTiO_3$ was improved by only the ultra-miniaturization of the cocatalyst. This effect of ultra-miniaturization of the cocatalyst is different from that found for the $Au_{25}/BaLa_4Ti_4O_{15}$ system, suggesting that the effect of ultra-miniaturization of the cocatalyst depends on the photocatalyst.

2. Experimental

2.1. Chemicals

All chemicals were commercially obtained and used without further purification. Hydrogen tetrachloroaurate tetrahydrate ($HAuCl_4 \cdot 4H_2O$) was purchased from Tanaka Kikinzoku. Tetraoctylammonium bromide, triphenylphosphine ($(C_6H_5)_3P$), glutathione (GSH), sodium tetrahydroborate, bismuth standard solution (100 ppm), gold standard solution (1000 ppm), and strontium titanate ($SrTiO_3$) were obtained from Wako Pure Chemical Industries. Methanol, toluene, acetone, ethanol, hexane, and chloroform were purchased from Kanto Chemical. Pure Milli-Q water (18.2 MΩ·cm) was obtained using a Merck Millipore Direct 3 UV system.

2.2. Preparation of $Au_{25}/SrTiO_3$

Glutathionate (SG)-protected Au_{25} clusters ($Au_{25}(SG)_{18}$; Scheme 2(b))[16] were used as the cocatalyst precursor because their size-selective synthesis has been well established. Loading of the Au_{25}-cluster cocatalyst on $SrTiO_3$ was conducted by the method illustrated in Scheme 1(b).

***Synthesis of $Au_{25}(SG)_{18}$*:** $Au_{25}(SG)_{18}$ was synthesized by the conversion of $(C_6H_5)_3P$-protected Au_n clusters into $Au_{25}(SG)_{18}$ through a ligand-exchange reaction.[46] The $(C_6H_5)_3P$-protected Au_n clusters were prepared by a procedure similar to that reported previously.[47] Chloroform (75 mL) containing $(C_6H_5)_3P$-protected Au_n clusters (50.4 mg) was mixed with water (75 mL) containing GSH (1456.5 mg, 4.7 mmol). The mixture was heated under reflux at 60 °C for about 10 h. The aqueous phase was then separated from the chloroform phase using a separation funnel. $Au_{25}(SG)_{18}$ was obtained by removing excess GSH by ultrafiltration of the aqueous phase.

***Loading of Au_{25}-cluster cocatalyst onto $SrTiO_3$*:** First, $Au_{25}(SG)_{18}$ clusters were adsorbed on $SrTiO_3$ by mixing an aqueous solution containing $Au_{25}(SG)_{18}$ with an aqueous solution of $SrTiO_3$ (600 mg) for 2 h at room temperature (Scheme 1(b)). The total volume of aqueous solution was fixed at 200 mL, and the mixing ratio of

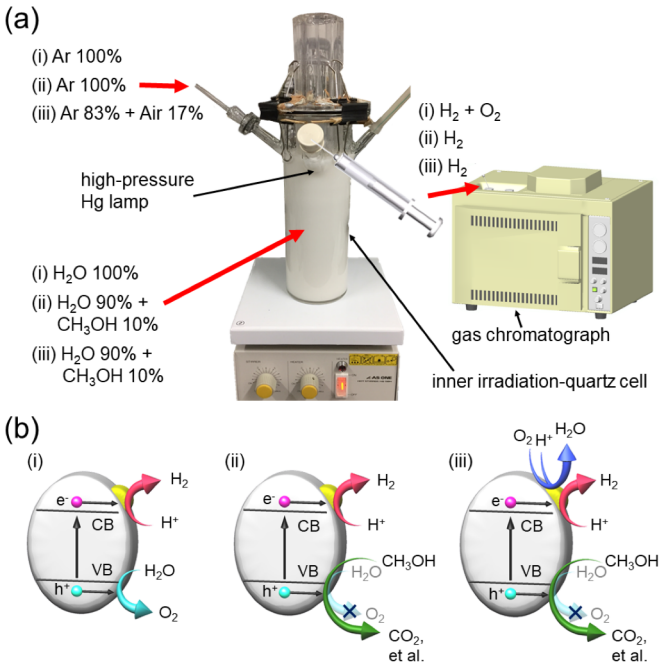

Figure 1. (a) Experimental conditions and (b) schematics of reactions; (i) photocatalytic water splitting, and photocatalytic H_2 evolution using methanol as a sacrificial reagent under a flow of (ii) Ar gas (namely, without O_2 in the reaction system) and (iii) a 5:1 mixture of Ar to air (namely, with O_2 in the reaction system).

$Au_{25}(SG)_{18}$ cluster to $SrTiO_3$ was fixed at 0.1 wt% Au because it gave a photocatalyst that showed high activity in the study on $Au_{25}/BaLa_4Ti_4O_{15}$.[41] The actual amount of Au adsorbed on $SrTiO_3$ was determined by inductively coupled plasma mass spectrometry (ICP-MS) analysis of each aqueous solution after mixing. The obtained $Au_{25}(SG)_{18}/SrTiO_3$ was calcined under reduced pressure (>1.0×10^{-1} Pa) at 300 °C for 2 h to provide $Au_{25}/SrTiO_3$ (Scheme 1(b)).

2.3. Preparation of Au Nanoparticle (Au_{NP})-loaded $SrTiO_3$ ($Au_{NP}/SrTiO_3$)

For comparison, $Au_{NP}/SrTiO_3$ was prepared using a conventional photodeposition method. First, $SrTiO_3$ (600 mg) was added to aqueous $HAuCl_4$ solution (350 mL) in a quartz cell. The gold content was fixed at 0.1 wt%. The mixture was stirred for 1 h at room temperature and then irradiated with a high-pressure Hg lamp (400 W) for 1 h. The average diameter of the particles loaded onto $SrTiO_3$ was estimated to be 9.5±3.3 nm by transmission electron microscopy (TEM).

2.4. Measurement of Photocatalytic Activity

In the following experiments, the evolved gases were analyzed by gas chromatography (Shimadzu GC-8A equipped with a thermal conductivity detector and 5A molecular sieve column; Ar carrier gas).

***Water Splitting*:** The photocatalytic water-splitting reaction by the photocatalysts ($Au_{25}/SrTiO_3$ and $Au_{NP}/SrTiO_3$) was performed at room temperature using an experimental apparatus built in-house that consisted of a high-pressure Hg lamp (400 W) and quartz cell (Figure 1). The reaction was conducted under Ar gas at a flow rate of 30 mL/min ((i) in Figure 1). Before the measurements, the reaction solution consisting of a prepared photocatalyst (500 mg) in water (350 mL) was purged with Ar gas for 1 h to ensure complete removal of air from the reaction vessel.

***Hydrogen Evolution using a Sacrificial Reagent*:** In this experiment, the H_2-evolution ability of the photocatalysts ($Au_{25}/SrTiO_3$ and $Au_{NP}/SrTiO_3$) was estimated using methanol as a sacrificial reagent ((ii) in Figure 1). Methanol (CH_3OH) solution (10%, 350 mL) containing a photocatalyst (500 mg) was irradiated with a high-pressure Hg lamp (400 W) under an Ar flow of 30 mL/min at room temperature.

***Oxygen Photoreduction*:** In this experiment, the decrease of the quantity of evolved H_2 was examined to investigate the likelihood of the oxygen (O_2)-photoreduction reaction. In particular, the H_2-evolution ability (see the above section) of the photocatalysts ($Au_{25}/SrTiO_3$ and $Au_{NP}/SrTiO_3$) was examined in a gas mixture of 5:1 Ar to air instead of pure Ar ((iii) in Figure 1).

2.5. Characterization

The optical absorption spectrum of an aqueous solution of $Au_{25}(SG)_{18}$ cluster was recorded at ambient temperature with a JASCO V-630 spectrometer.

Diffuse reflectance (DR) spectra of $Au_{25}(SG)_{18}/SrTiO_3$, $Au_{25}/SrTiO_3$, and $Au_{NP}/SrTiO_3$ were acquired at ambient temperature using a JASCO V-670 spectrometer.

ICP-MS was conducted using an Agilent 7500c spectrometer (Agilent Technologies, Tokyo, Japan). Bi was used as an internal standard. The ICP-MS measurements were conducted for the solution after mixing to estimate the quantity of Au that was not adsorbed on $SrTiO_3$. The adsorption efficiency was estimated on the basis of that value.

TEM images were recorded with a Hitachi H-9500 electron microscope operating at 200 kV, typically using a magnification of ×150,000, or a JEOL JEM-2100 electron microscope operating at 200 kV, typically using a magnification of ×600,000.

X-ray photoelectron spectra were recorded using a JEOL JPS-9010MC electron spectrometer equipped with a chamber at a base pressure of ~2×10^{-8} Torr. X-rays from the Mg Kα line at 1253.6 eV were used for excitation. The binding energies were corrected by calibrating the binding energy of Ti $2p_{3/2}$ in $SrTiO_3$, which was determined before this study.

Powder X-ray diffraction (XRD) measurements were performed on a Rigaku Rint2500 diffractometer using Cu Kα radiation (λ = 1.5418 Å). A reflection-free silicon plate was used as a substrate.

Scanning electron microscopy (SEM) images were recorded with a JEOL JSM-7600F electron microscope operating at 200 kV, typically using a magnification of ×40,000.

3. Results and Discussion

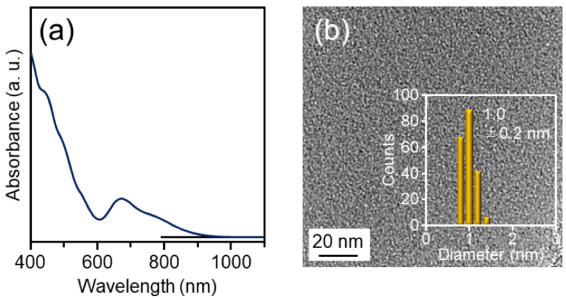

Figure 2. (a) Optical absorption spectrum and (b) TEM image and associated particle-size distribution of $Au_{25}(SG)_{18}$.

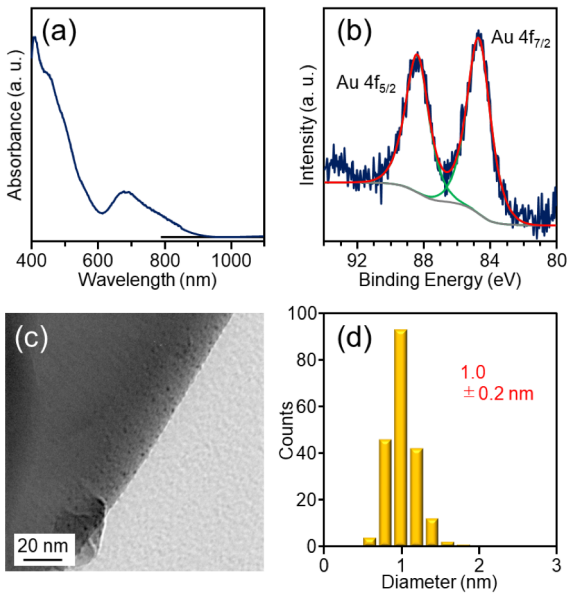

Figure 3. (a) DR spectrum, (b) Au 4f spectrum, (c) TEM image, and (d) particle-size distribution of $Au_{25}(SG)_{18}/SrTiO_3$.

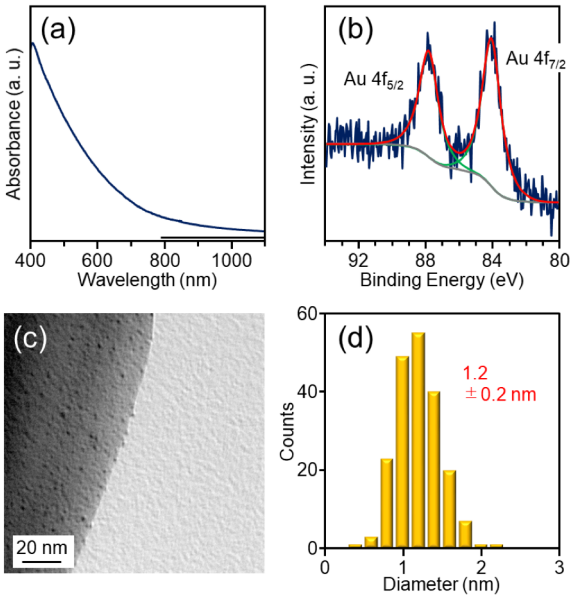

Figure 4. (a) DR spectrum, (b) Au 4f spectrum, (c) TEM image, and (d) particle-size distribution of $Au_{25}/SrTiO_3$.

3.1. Loading of Au_{25}-cluster cocatalyst onto $SrTiO_3$

The $Au_{25}(SG)_{18}$ cluster (Figure 2(a)) synthesized in this study demonstrated similar optical absorption features to that reported previously.[16] The TEM image of $Au_{25}(SG)_{18}$ only contained ~1-nm particles (Figure 2(b)). These results demonstrate that the $Au_{25}(SG)_{18}$ cluster synthesized in this study was of high purity.

The $Au_{25}(SG)_{18}$ cluster was adsorbed on $SrTiO_3$ with an adsorption ratio of 99.8% by stirring with $SrTiO_3$ in water (see Section 2.2). Hydroxyl (-OH) groups are presumed to be present on the surface of $SrTiO_3$ in H_2O. It is interpreted that $Au_{25}(SG)_{18}$ is adsorbed on $SrTiO_3$ with a high adsorption ratio because the polar functional groups (-CO_2H and NH_2) of SG form hydrogen bonds with these -OH groups.

Figure 3(a) shows the DR spectrum of $Au_{25}(SG)_{18}/SrTiO_3$. A characteristic peak of $Au_{25}(SG)_{18}$ (Figure 2(a)) appears in the DR spectrum. In the Au 4f spectrum of $Au_{25}(SG)_{18}/SrTiO_3$, peaks attributable to Au were observed at binding energies of 84.7 and 88.4 eV (Figure 3(b)). These peak positions are in good agreement with those observed in the Au 4f spectrum of $Au_{25}(SG)_{18}$ (84.7 and 88.5 eV).[16] Only particles with a diameter of ~1 nm were observed in the TEM image of $Au_{25}(SG)_{18}/SrTiO_3$ (Figure 3(c) and (d)). These results indicate that $Au_{25}(SG)_{18}$ was adsorbed on $SrTiO_3$ without deterioration.

Figure 4(a) shows the DR spectrum of the photocatalyst after calcination ($Au_{25}/SrTiO_3$). This spectrum lacks the characteristic peak of $Au_{25}(SG)_{18}$ and absorption gradually increases from the long wavelength side to the short wavelength side. These results indicate that the geometric structure of $Au_{25}(SG)_{18}$ was remarkably changed by calcination. In the Au 4f spectrum of $Au_{25}/SrTiO_3$, peaks attributable to Au were observed at binding energies of 84.1 and 87.9 eV (Figure 4(b)). These peak positions are shifted to lower energy compared with those of $Au_{25}(SG)_{18}/SrTiO_3$ (84.7 and 88.4 eV; Figure 3(b)) and are close to those of bulk Au (84.0 and 87.7 eV[48]). These results suggest that the SG ligand was removed by calcination. In fact, almost no peak was observed in the S 2p spectrum of $Au_{25}/SrTiO_3$. The TEM image of $Au_{25}/SrTiO_3$ (Figure 4(c)) only contained ~1.2-nm particles (Figure 4(d)). The slight increase of particle size is attributed to the structural change induced by the removal of the SG ligands.[41,42,49] These results indicate that no substantial cluster aggregation occurred upon ligand removal. This interpretation was also supported by the fact that almost no ~520-nm plasmon peak, which would indicate the presence of Au_{NP} of 2 nm or larger,[50] was observed in the DR spectrum (Figure 4(a)).

Figure 5 shows the powder XRD patterns and SEM images of $SrTiO_3$,[51] $Au_{25}(SG)_{18}/SrTiO_3$, and $Au_{25}/SrTiO_3$. The XRD patterns and SEM images of the respective samples are extremely similar. These results indicate that the crystal structure of $SrTiO_3$ is maintained after the adsorption of $Au_{25}(SG)_{18}$ and the subsequent removal of the SG ligands.

All of these results confirmed that extremely fine Au-cocatalyst particles (Au_{25} clusters) were precisely loaded on the $SrTiO_3$ water-splitting photocatalyst using the method summarized in Scheme 1(b). This means that the loading method to support ultrafine Au-cocatalyst particles on a photocatalyst presented in Scheme 1(b) is relatively versatile.

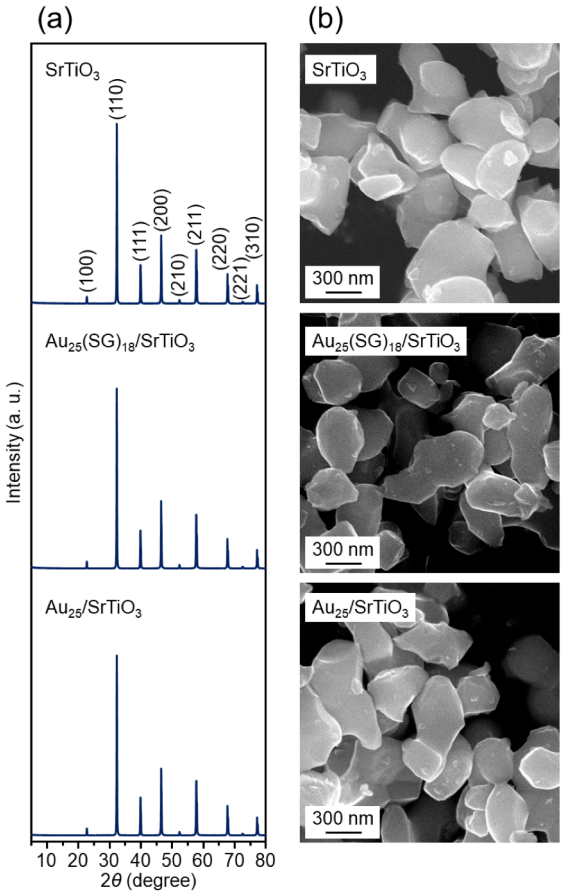

Figure 5. (a) XRD patterns and (b) SEM images for $SrTiO_3$,[51] $Au_{25}(SG)_{18}/SrTiO_3$, and $Au_{25}/SrTiO_3$.

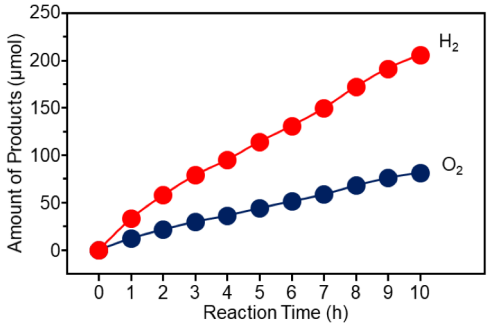

Figure 6. Time course of water splitting over $Au_{25}/SrTiO_3$ (0.1 wt% Au).

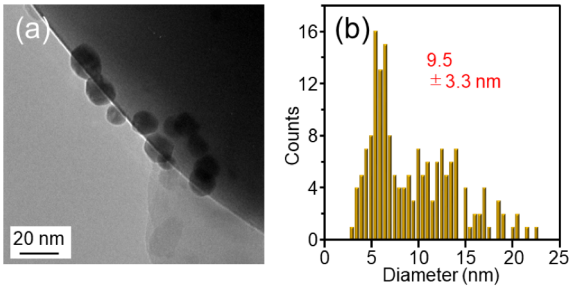

Figure 7. (a) TEM image and (b) associated particle-size distribution of $Au_{NP}/SrTiO_3$.

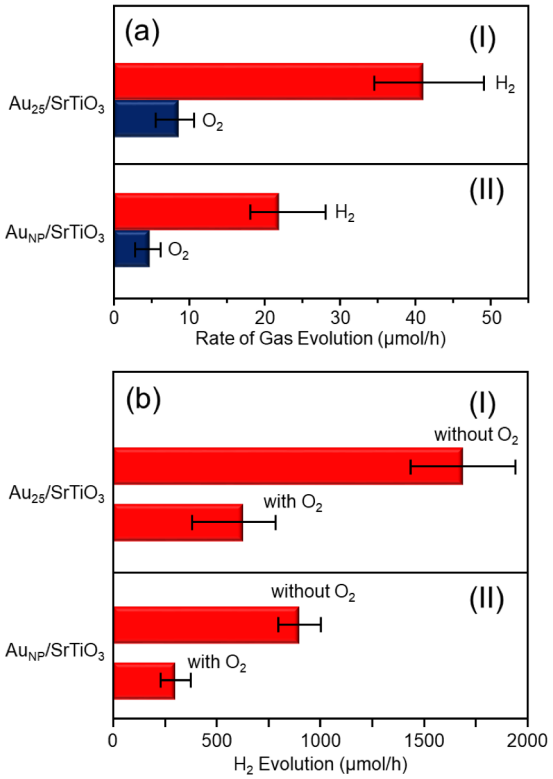

Figure 8. Comparison of the rates of photocatalytic evolution of (a) H_2 and O_2 by water splitting and (b) H_2 using methanol as a sacrificial reagent under a flow of Ar gas (labeled "without O_2") or 5:1 mixture of Ar to air (labeled "with O_2") by (I) $Au_{25}/SrTiO_3$ and (II) $Au_{NP}/SrTiO_3$. Averages of the values obtained from several experiments are displayed.

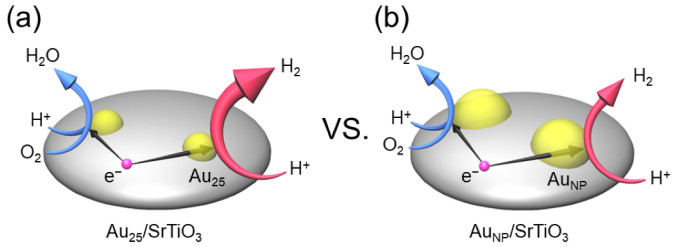

Figure 9. Schematic of the effect of ultra-miniaturization of the Au cocatalyst on H_2 evolution and the O_2-photoreduction reaction; (a) $Au_{25}/SrTiO_3$ and (b) $Au_{NP}/SrTiO_3$.

3.2. Effect of refining the cocatalyst on photocatalytic activity

The $Au_{25}/SrTiO_3$ thus obtained catalyzed the water-splitting reaction under UV-light irradiation. Figure 6 shows the time course of the amount of gas evolved. This amount continuously increased over time. However, the ratio of the generated H_2 and O_2 was not 2:1 in this water-splitting reaction. Domen et al.[52] reported that it is difficult for oxidized species to detach as O_2 from the surface of $SrTiO_3$. This might be the reason why the amount of O_2 generated was slightly smaller than the 2:1 stoichiometric ratio of the water-splitting reaction using $Au_{25}/SrTiO_3$. This phenomenon was also observed for the water-splitting reaction using $Au_{NP}/SrTiO_3$.

We compared the amounts of gas generated over $Au_{25}/SrTiO_3$ and $Au_{NP}/SrTiO_3$ (Figure 7) to investigate the effect of ultra-miniaturization of the Au cocatalyst on the water-splitting activity of $SrTiO_3$. Figure 8(a)(I) and (II) show the amounts of gas evolved during the first hour when $Au_{25}/SrTiO_3$ and $Au_{NP}/SrTiO_3$, respectively, were used for the photocatalyst. Figure 8(a) reveals that $Au_{25}/SrTiO_3$ produced approximately twice as much gas (41.2 μmol/h of H_2) as $Au_{NP}/SrTiO_3$ (21.9 μmol/h of H_2). These results indicate that ultra-miniaturization of the cocatalyst increases the water-splitting activity of Au-loaded $SrTiO_3$.

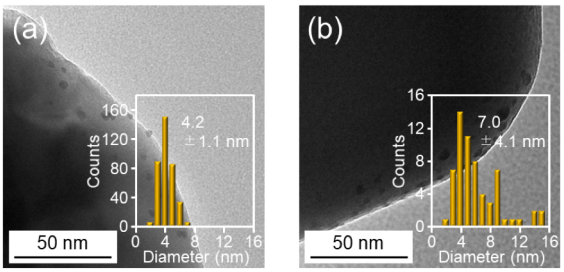

Figure 10. Comparison of TEM images and associated particle-size distributions of (a) $Au_{25}/SrTiO_3$ and (b) $Au_{25}/BaLa_4Ti_4O_{15}$ after UV irradiation for 10 h.

To investigate the origin of the improved water-splitting activity caused by the ultra-miniaturization of the Au cocatalyst, we examined the effect of refining the cocatalyst on each reaction occurring on the photocatalyst. When CH_3OH is present in the solution, holes generated by photoexcitation are used in decomposition of CH_3OH rather than O_2 production ((ii) in Figure 1(b)).[3] Under these conditions, the production of O_2 is negligible and therefore the inhibition reaction involving O_2 hardly occurs.[43,53,54] That is, evaluating the H_2-production ability of the cocatalyst ((ii) in Figure 1(b)) is possible under these conditions ((ii) in Figure 1(a)). Figure 8(b) shows the amount of H_2 generated during the first 1 hour under these conditions (without O_2). $Au_{25}/SrTiO_3$ generated approximately twice as much H_2 (1689 μmol/h) as $Au_{NP}/SrTiO_3$ (899 μmol/h). This comparison indicates that ultra-miniaturization of the Au cocatalyst promotes the H_2-formation reaction (Figure 9).

We also investigated the effect of Au cocatalyst ultra-miniaturization on the other reaction. Previous studies demonstrated that the Au cocatalyst prevented the back reaction in the absence of light irradiation, whereas the inhibition reaction related to the reduction of O_2 (hereafter termed the O_2-photoreduction reaction) occurs under light irradiation.[53,54] Therefore, in this experiment, we investigated the effect of cocatalyst ultra-miniaturization on the O_2-photoreduction reaction. In the experiments, O_2 was included in the flowing gas ((iii) in Figure 1 (a)) to promote the O_2-photoreduction reaction. Figure 8(b) shows the amount of H_2 generated during the first 1 hour in the presence of O_2. Over both $Au_{25}/SrTiO_3$ and $Au_{NP}/SrTiO_3$, the amount of H_2 evolved was greatly decreased compared with the cases where O_2 was not present. This behavior indicates that the O_2-photoreduction reaction proceeds under light irradiation for both photocatalysts. Regarding the decrease ratio of the amount of H_2 produced, similar ratios of 39% and 34% were observed for $Au_{25}/SrTiO_3$ and $Au_{NP}/SrTiO_3$, respectively. This result means that the O_2-photoreduction reaction occurs to the same extent for both photocatalysts. In other words, the ultra-miniaturization of the Au cocatalyst does not strongly affect the likelihood of the O_2-photoreduction reaction (Figure 9).

These results show that for Au-loaded $SrTiO_3$, ultra-miniaturization of the cocatalyst accelerates the H_2-formation reaction without strongly affecting the O_2-photoreduction reaction. Thus, it can be concluded that the improvement of the water-splitting activity induced by ultra-miniaturization of the cocatalyst is mainly caused by the acceleration of the H_2-formation reaction.

This effect of ultra-miniaturization of the Au cocatalyst differs from that found for Au-loaded $BaLa_4Ti_4O_{15}$; in the case of Au-loaded $BaLa_4Ti_4O_{15}$, the refinement of the cocatalyst enhanced both the H_2-evolution reaction and the O_2-photoreduction reaction and thereby the water-splitting activity was not improved through only the ultra-miniaturization of the cocatalyst.[43] The differences in the effect of refining the cocatalyst are presumed to be related to differences in the binding mode between the cocatalyst and photocatalyst, the magnitude of charge transfer, and/or the geometric/electronic structures of the cocatalyst between Au-loaded $SrTiO_3$ and Au-loaded $BaLa_4Ti_4O_{15}$. In fact, although an increase in the cocatalyst particle diameter was observed for both of the photocatalysts after 10 h of reaction, the increase in the cocatalyst particle size in $Au_{25}/SrTiO_3$ was not as large as that in $Au_{25}/BaLa_4Ti_4O_{15}$ (Figure 10). Thus, it is presumed that a stronger bond is formed between the cocatalyst and photocatalyst in $Au_{25}/SrTiO_3$ than in $Au_{25}/BaLa_4Ti_4O_{15}$. In the future, it is expected that further information about the binding mode between the cocatalyst and photocatalyst, magnitude of charge transfer, and geometric/electronic structures of the cocatalyst will be obtained by high-resolution measurements[49,55,56] and theoretical calculations,[57] thereby providing a deeper understanding of the reasons why the effect of cocatalyst ultra-miniaturization depends on the photocatalyst.

4. Conclusion

This study elucidated that when using $SrTiO_3$ as the photocatalyst, the size of the Au cocatalyst can be strictly controlled within the ultrafine regime by using a thiolate-protected Au cluster as the precursor. It was also revealed that in the Au-loaded $SrTiO_3$, ultra-miniaturization of the cocatalyst increased the water-splitting activity. It was concluded that this improvement in activity is mainly caused by the acceleration of the H_2-formation reaction. The effect of ultra-miniaturization of the cocatalyst observed herein is different from that observed for Au-loaded $BaLa_4Ti_4O_{15}$. Thus, it became clear that the effects of refining the cocatalyst depend on the underlying photocatalyst. These findings are expected to lead to more elaborate design guidelines for higher functionalization of water-splitting semiconductor photocatalysts.

5. Acknowledgments

We thank Ms. Rui Hayashi and Mr. Kosuke Wakamatsu (Tokyo University of Science) for technical assistance and Prof. Akihiko Kudo and Dr. Akihide Iwase (Tokyo University of Science) for valuable discussions. This work was supported by the Japan Society for the Promotion of Science (JSPS) KAKENHI (grant number JP16H04099, JP17H05385, and JP16K21402), and Scientific Research on Innovative Areas “All Nippon Artificial Photosynthesis Project for Living Earth (AnApple)” (grant number 15H00883). Funding from the Takahashi Industrial and Economic Research Foundation, Futaba Electronics Memorial Foundation, Iwatani Naoji Foundation, and Ube Industries Foundation is also gratefully acknowledged.

6. References

[1] Fujishima, A.; Honda, K. Electrochemical Photolysis of Water at a Semiconductor Electrode. *Nature* **1972**, *238*, 37–38.

[2] Maeda, K.; Domen, K. Photocatalytic Water Splitting: Recent Progress and Future Challenges. *J. Phys. Chem. Lett.* **2010**, *1*, 2655−2661.

[3] Kudo, A.; Miseki, Y. Heterogeneous Photocatalyst Materials for Water Splitting. *Chem. Soc. Rev.* **2009**, *38*, 253–278.

[4] Abe, R. Development of a New System for Photocatalytic Water Splitting into H_2 and O_2 under Visible Light Irradiation. *Bull. Chem. Soc. Jpn.* **2011**, *84*, 1000−1030.

[5] Maeda, K. Z-Scheme Water Splitting Using Two Different Semiconductor Photocatalysts. *ACS Catal.* **2013**, *3*, 1486−1503.

[6] Miseki, Y.; Fujiyoshi, S.; Gunji, T.; Sayama, K. Photocatalytic Z-Scheme Water Splitting for Independent H_2/O_2 Production via a Stepwise Operation Employing a Vanadate Redox Mediator under Visible Light. *J. Phys. Chem. C* **2017**, *121*, 9691−9697.

[7] Osterloh, F. E. Inorganic Materials as Catalysts for Photochemical Splitting of Water. *Chem. Mater.* **2008**, *20*, 35–54.

[8] Li, X.; Yu, J.; Low, J.; Fang, Y.; Xiao, J.; Chen, X. Engineering Heterogeneous Semiconductors for Solar Water Splitting. *J. Mater. Chem. A* **2015**, *3*, 2485–2534.

[9] Mallouk, T. E. The Emerging Technology of Solar Fuels. *J. Phys. Chem. Lett.* **2010**, *1*, 2738–2739.

[10] Ida, S.; Okamoto, Y.; Matsuka, M.; Hagiwara, H.; Ishihara, T. Preparation of Tantalum-Based Oxynitride Nanosheets by Exfoliation of a Layered Oxynitride, $CsCa_2Ta_3O_{10-x}N_y$, and Their Photocatalytic Activity. *J. Am. Chem. Soc.* **2012**, *134*, 15773–15782.

[11] Iwase, A.; Ng, Y. H.; Ishiguro, Y.; Kudo, A.; Amal, R. Reduced Graphene Oxide as a Solid-State Electron Mediator in Z-Scheme Photocatalytic Water Splitting under Visible Light. *J. Am. Chem. Soc.* **2011**, *133*, 11054–11057.

[12] Maeda, K.; Teramura, K.; Lu, D.; Saito, N.; Inoue, Y.; Domen, K. Noble-Metal/Cr_2O_3 Core/Shell Nanoparticles as a Cocatalyst for Photocatalytic Overall Water Splitting. *Angew. Chem., Int. Ed.* **2006**, *45*, 7806−7809.

[13] Takata, T.; Pan, C.; Nakabayashi, M.; Shibata, N.; Domen, K. Fabrication of a Core−Shell-Type Photocatalyst via Photodeposition of Group IV and V Transition Metal Oxyhydroxides: An Effective Surface Modification Method for Overall Water Splitting. *J. Am. Chem. Soc.* **2015**, *137*, 9627−9634.

[14] Pan, C.; Takata, T.; Nakabayashi, M.; Matsumoto, T.; Shibata, N.; Ikuhara, Y.; Domen, K. A Complex Perovskite-Type Oxynitride: The First Photocatalyst for Water Splitting Operable at up to 600 nm. *Angew. Chem., Int. Ed.* **2015**, *54*, 2955−2959.

[15] Garcia-Esparza, A. T.; Shinagawa, T.; Ould-Chikh, S.; Qureshi, M.; Peng, X.; Wei, N.; Anjum, D. H.; Clo, A.; Weng, T.-C.; Nordlund, D.; Sokaras, D.; Kubota, J.; Domen, K.; Takanabe, K. An Oxygen-Insensitive Hydrogen Evolution Catalyst Coated by a Molybdenum-Based Layer for Overall Water Splitting. *Angew. Chem., Int. Ed.* **2017**, *56*, 5780–5784.

[16] Negishi, Y.; Nobusada, K.; Tsukuda, T. Glutathione-Protected Gold Clusters Revisited: Bridging the Gap between Gold(I)–Thiolate Complexes and Thiolate-Protected Gold Nanocrystals. *J. Am. Chem. Soc.* **2005**, *127*, 5261–5270.
[17] Tsukuda, T. Toward an Atomic-Level Understanding of Size-Specific Properties of Protected and Stabilized Gold Clusters. *Bull. Chem. Soc. Jpn.* **2012**, *85*, 151–168.
[18] Jin, R.; Zeng, C.; Zhou, M.; Chen, Y. Atomically Precise Colloidal Metal Nanoclusters and Nanoparticles: Fundamentals and Opportunities. *Chem. Rev.* **2016**, *116*, 10346–10413.
[19] Zhu, M.; Aikens, C. M.; Hollander, F. J.; Schatz, G. C.; Jin, R. Correlating the Crystal Structure of A Thiol-Protected Au_{25} Cluster and Optical Properties. *J. Am. Chem. Soc.* **2008**, *130*, 5883–5885.
[20] Häkkinen, H. The Gold-Sulfur Interface at the Nanoscale. *Nat. Chem.* **2012**, *4*, 443–455.
[21] Kurashige, W.; Niihori, Y.; Sharma, S.; Negishi, Y. Precise Synthesis, Functionalization and Application of Thiolate-Protected Gold Clusters. *Coord. Chem. Rev.* **2016**, *320–321*, 238–250.
[22] Black, D. M.; Bhattarai, N.; Bach, S. B. H.; Whetten, R. L. Selection and Identification of Molecular Gold Clusters at the Nano(gram) Scale: Reversed Phase HPLC−ESI−MS of a Mixture of Au-Peth MPCs. *J. Phys. Chem. Lett.* **2016**, *7*, 3199–3205.
[23] Yu, Y.; Luo, Z.; Chevrier, D. M.; Leong, D. T.; Zhang, P.; Jiang, D.-E.; Xie, J. Identification of a Highly Luminescent $Au_{22}(SG)_{18}$ Nanocluster. *J. Am. Chem. Soc.* **2014**, *136*, 1246–1249.
[24] Antonello, S.; Dainese, T.; Pan, F.; Rissanen, K.; Maran, F. Electrocrystallization of Monolayer-Protected Gold Clusters: Opening the Door to Quality, Quantity, and New Structures. *J. Am. Chem. Soc.* **2017**, *139*, 4168–4174.
[25] Kwak, K.; Choi, W.; Tang, Q.; Kim, M.; Lee, Y.; Jiang, D.-E.; Lee, D. A Molecule-Like $PtAu_{24}(SC_6H_{13})_{18}$ Nanocluster as an Electrocatalyst for Hydrogen Production. *Nat. Commun.* **2017**, *8*, 14723.
[26] Knoppe, S.; Bürgi, T. Chirality in Thiolate-Protected Gold Clusters. *Acc. Chem. Res.* **2014**, *47*, 1318–1326.
[27] Liu, P.; Qin, R.; Fu, G.; Zheng, N. Surface Coordination Chemistry of Metal Nanomaterials. *J. Am. Chem. Soc.* **2017**, *139*, 2122–2131.
[28] Heinecke, C. L.; Ni, T. W.; Malola, S.; Mäkinen, V.; Wong, O. A.; Häkkinen, H.; Ackerson, C. J. Structural and Theoretical Basis for Ligand Exchange on Thiolate Monolayer Protected Gold Nanoclusters. *J. Am. Chem. Soc.* **2012**, *134*, 13316–13322
[29] Konishi, K.; Iwasaki, M.; Sugiuchi, M.; Shichibu, Y. Ligand-Based Toolboxes for Tuning of the Optical Properties of Subnanometer Gold Clusters. *J. Phys. Chem. Lett.* **2016**, *7*, 4267−4274.
[30] Joshi, C. P.; Bootharaju, M. S.; Alhilaly, M. J.; Bakr, O. M. $[Ag_{25}(SR)_{18}]^-$: The "Golden" Silver Nanoparticle. *J. Am. Chem. Soc.* **2015**, *137*, 11578–11581.
[31] Sakthivel, N. A.; Theivendran, S.; Ganeshraj, V.; Oliver, A. G.; Dass, A. Crystal Structure of Faradaurate-279: $Au_{279}(SPh\text{-}tBu)_{84}$ Plasmonic Nanocrystal Molecules. *J. Am. Chem. Soc.* **2017**, *139*, 15450–15459.
[32] Chakraborty, I.; Pradeep, T. Atomically Precise Clusters of Noble Metals: Emerging Link between Atoms and Nanoparticles. *Chem. Rev.* **2017**, *117*, 8208–8271.
[33] Fernando, A.; Weerawardene, K. L. D. M.; Karimova, N. V.; Aikens, C. M. Quantum Mechanical Studies of Large Metal, Metal Oxide, and Metal Chalcogenide Nanoparticles and Clusters. *Chem. Rev.* **2015**, *115*, 6112–6216.
[34] Tang, Q.; Jiang, D.-E. Computational Insight into the Covalent Organic−Inorganic Interface. *Chem. Mater.* **2016**, *28*, 5976–5988.
[35] Yang, S.; Chai, J.; Song, Y.; Fan, J.; Chen, T.; Wang, S.; Yu, H.; Li, X.; Zhu, M. In Situ Two-Phase Ligand Exchange: A New Method for the Synthesis of Alloy Nanoclusters with Precise Atomic Structures. *J. Am. Chem. Soc.* **2017**, *139*, 5668–5671.
[36] Liao, L.; Zhuang, S.; Yao, C.; Yan, N.; Chen, J.; Wang, C.; Xia, N.; Liu, X.; Li, M.-B.; Li, L.; Bao, X.; Wu, Z. Structure of Chiral $Au_{44}(2,4\text{-}DMBT)_{26}$ Nanocluster with an 18-Electron Shell Closure. *J. Am. Chem. Soc.* **2016**, *138*, 10425–10428.
[37] Sakamoto, N.; Ohtsuka, H.; Ikeda, T.; Maeda, K.; Lu, D.; Kanehara, M.; Teramura, K.; Teranishi, T.; Domen, K. Highly Dispersed Noble-Metal/Chromia (Core/Shell) Nanoparticles as Efficient Hydrogen Evolution Promoters for Photocatalytic Overall Water Splitting under Visible Light. *Nanoscale* **2009**, *1*, 106–109.
[38] Maeda, K.; Sakamoto, N.; Ikeda, T.; Ohtsuka, H.; Xiong, A.; Lu, D.; Kanehara, M.; Teranishi, T.; Domen, K. Preparation of Core–Shell-Structured Nanoparticles (with a Noble-Metal or Metal Oxide Core and a Chromia Shell) and Their Application in Water Splitting by Means of Visible Light. *Chem.–Eur. J.* **2010**, *16*, 7750–7759.
[39] Ikeda, T.; Xiong, A.; Yoshinaga, T.; Maeda, K.; Domen, K.; Teranishi, T. Polyol Synthesis of Size-Controlled Rh Nanoparticles and Their Application to Photocatalytic Overall Water Splitting under Visible Light. *J. Phys. Chem. C* **2013**, *117*, 2467–2473.

[40] Miseki, Y.; Kato, H.; Kudo, A. Water Splitting into H_2 and O_2 over Niobate and Titanate Photocatalysts with (111) Plane-Type Layered Perovskite Structure. *Energy Environ. Sci.* **2009**, *2*, 306−314.
[41] Negishi, Y.; Mizuno, M.; Hirayama, M.; Omatoi, M.; Takayama, T.; Iwase, A.; Kudo, A. Enhanced Photocatalytic Water Splitting by $BaLa_4Ti_4O_{15}$ Loaded with ~1 nm Gold Nanoclusters Using Glutathione-Protected Au_{25} Clusters. *Nanoscale* **2013**, *5*, 7188–7192.
[42] Negishi, Y.; Matsuura, Y.; Tomizawa, R.; Kurashige, W.; Niihori, Y.; Takayama, T.; Iwase, A.; Kudo, A. Controlled Loading of Small Au_n Clusters (n = 10−39) onto $BaLa_4Ti_4O_{15}$ Photocatalysts: Toward an Understanding of Size Effect of Cocatalyst on Water-Splitting Photocatalytic Activity. *J. Phys. Chem. C* **2015**, *119*, 11224−11232.
[43] Kurashige, W.; Kumazawa, R.; Ishii, D.; Hayashi, R.; Niihori, Y.; Hossain, S.; Nair, L. V.; Takayama, T.; Iwase, A.; Yamazoe, S.; Tsukuda, T.; Kudo, A.; Negishi, Y. *Submitted*.
[44] Tomio, T.; Miki, H.; Tabata, H.; Kawai, T.; Kawai, S. Control of Electrical Conductivity in Laser Deposited $SrTiO_3$ Thin Films with Nb Doping. *J. Appl. Phys.* **1994**, 76, 5886−5890.
[45] Puangpetch, T.; Chavadej, S.; Sreethawong, T. Hydrogen Production over Au-Loaded Mesoporous-Assembled $SrTiO_3$ Nanocrystal Photocatalyst: Effects of Molecular Structure and Chemical Properties of Hole Scavengers. *Energ. Convers. Manage.* **2011**, *52*, 2256–2261.
[46] Shichibu, Y.; Negishi, Y.; Tsukuda, T.; Teranishi, T. Large-Scale Synthesis of Thiolated Au_{25} Clusters via Ligand Exchange Reactions of Phosphine-Stabilized Au_{11} Clusters. *J. Am. Chem. Soc.* **2005**, *127*, 13464–13465.
[47] Qian, H.; Eckenhoff, W. T.; Bier, M. E.; Pintauer, T.; Jin, R. Crystal Structures of Au_2 Complex and Au_{25} Nanocluster and Mechanistic Insight into the Conversion of Polydisperse Nanoparticles into Monodisperse Au_{25} Nanoclusters. *Inorg. Chem.* **2011**, *50*, 10735–10739.
[48] Fu, S.; Fan, G.; Yang, L.; Li, F. Non-Enzymatic Glucose Sensor Based on Au Nanoparticles Decorated Ternary Ni-Al Layered Double Hydroxide/Single-Walled Carbon Nanotubes/Graphene Nanocomposite. *Electrochim. Acta* **2015**, *152*, 146−154.
[49] Bruma, A.; Negreiros, F. R.; Xie, S.; Tsukuda, T.; Johnston, R. L.; Fortunelli, A.; Li, Z. Y. Direct Atomic Imaging and Density Functional Theory Study of the $Au_{24}Pd_1$ Cluster Catalyst. *Nanoscale* **2013**, *5*, 9620–9625.
[50] Negishi, Y.; Nakazaki, T.; Malola, S.; Takano, S.; Niihori, Y.; Kurashige, W.; Yamazoe, S.; Tsukuda, T.; Häkkinen, H. A Critical Size for Emergence of Nonbulk Electronic and Geometric Structures in Dodecanethiolate-Protected Au Clusters. *J. Am. Chem. Soc.* **2015**, *137*, 1206–1212.
[51] Yang, Y.; Cheng, Y. F. Bi-Layered $CeO_2/SrTiO_3$ Nanocomposite Photoelectrode for Energy Storage and Photocathodic Protection. *Electrochim. Acta* **2017**, *253*, 134−141.
[52] Domen, K.; Naito, S.; Onishi, T.; Tamaru, K.; Soma, M. Study of the Photocatalytic Decomposition of Water Vapor over a $NiO–SrTiO_3$ Catalyst. *J. Phys. Chem.* **1982**, *86*, 3657–3661.
[53] Iwase, A.; Kato, H.; Kudo, A. Nanosized Au Particles as an Efficient Cocatalyst for Photocatalytic Overall Water Splitting. *Catal. Lett.* **2006**, *108*, 7–10.
[54] Iwase, A.; Kato, H.; Kudo, A. The Effect of Au Cocatalyst Loaded on La-Doped $NaTaO_3$ on Photocatalytic Water Splitting and O_2 Photoreduction. *Appl. Catal. B: Environ.* **2013**, *136–137*, 89–93.
[55] Yamazoe, S.; Takano, S.; Kurashige, W.; Yokoyama, T.; Nitta, K.; Negishi, Y.; Tsukuda, T. Hierarchy of Bond Stiffnesses within Icosahedral-Based Gold Clusters Protected by Thiolates. *Nat. Commun.* **2016**, *7*, 10414.
[56] Imaoka, T.; Akanuma, Y.; Haruta, N.; Tsuchiya, S.; Ishihara, K.; Okayasu, T.; Chun, W.-J.; Takahashi, M.; Yamamoto, K. Platinum Clusters with Precise Numbers of Atoms for Preparative-Scale Catalysis. *Nat. Commun.* **2017**, *8*, 688.
[57] Jiang, D.-E.; Overbury, S. H.; Dai, S. Interaction of Gold Clusters with a Hydroxylated Surface. *J. Phys. Chem. Lett.* **2011**, *2*, 1211–1215.